Single step processing of an integrated FGM BaTiO3-Ni capacitor for power modules' assembly

Romain Raisson, Sophie Guillemet-Fritsch, Pascal Dufour, Paul-Etienne Vidal, Geoffroy Chevallier, Donatien Martineau, Cyrille Duchesne

Single step processing of an integrated FGM BaTiO3-Ni capacitor for power modules' assembly

Romain Raisson, Sophie Guillemet-Fritsch, Pascal Dufour, Paul-Etienne Vidal, Geoffroy Chevallier, Donatien Martineau and Cyrille Duchesne

The first author is R. Raisson from UPPA, Avenue de l'Université 64012 Pau, France (romain.raisson@univ-pau.fr).
The second is S. Guillemet-Fritsch from CIRIMAT, Toulouse University 3 Paul Sabatier, Toulouse INP, CNRS, 118 Route de Narbonne, 31062 Toulouse cedex 9 – France (sophie.guillemet@univ-tlse3.fr)
The third is P. Dufour from CIRIMAT, Toulouse University 3 Paul Sabatier, Toulouse INP, CNRS, 118 Route de Narbonne, 31062 Toulouse cedex 9 – France (pascal.dufour@univ-tlse3.fr)
The fourth author is P.-E. Vidal from LGP, University of Technology of Tarbes and Toulouse University, 47 avenue d'Azereix, 65016 Tarbes, France (paul-etienne.vidal@uttop.fr) (Corresponding author).
The fifth is G. Chevallier from CIRIMAT, Toulouse University 3 Paul Sabatier, Toulouse INP, CNRS, 118 Route de Narbonne, 31062 Toulouse cedex 9 – France (geoffroy.chevallier@univ-tlse3.fr)
The sixth is D. Martineau from SAFRAN TECH, Rue des jeunes Bois, 78117 Châteaufort, France (donatien.martineau@safrangroup.com)
The seventh is C. Duchesne from DEEP CONCEPT, 2 Av. du Président Pierre Angot, 64000 Pau, France (cyrille.duchesne@deepconcept.fr)

Abstract— The miniaturization of power electronic devices is pushing manufacturers to improve the multifunctionality of components. Obtaining new materials with heterogeneous electrical properties is a challenge. In this work, the objective is to prepare, in a single step processing, a ceramic capacitor including a thick metallization. This device will be a first step towards its integration in a power module. The assembly of a metal and ceramics is a challenge due to the difference of properties of these materials. A new BaTiO3-Ni functionally graded material (FGM) has been obtained by SPS co-sintering. The processing parameters of the BaTiO3-Ni FGM are optimized to target highly dense material with controlled microstructure. In this case, a crack free device is obtained with controlled dielectric properties and can be integrated in a power module device. The processing leading to fabrication of this FGM in one step can be used for other components in power electronics applications.

Index Terms—Baryum Titanate oxide, Ceramic capacitor, Dielectric Material, Dielectric characterization, Microstructure, Nickel, Spark Plasma Sintering

I. INTRODUCTION

The need of more efficiency in power electronics applications as aeronautic and railway pushes the efforts of researchers towards the miniaturization of electronic components. In aeronautic and transport applications, power modules can deserve this purpose [1]. Power module package experiences high voltage (≥1kV) and high operating temperature (≥175°C). On the one hand, inside the power module assembly, most of parts and subcomponents close to the active chip must withstand such constraints. On the other hand, the miniaturization target requires optimized power modules' packages to target higher efficiency. Moreover, the use of Wide Band Gap semiconductors such as Silicon Carbide Metal Oxide Semiconductor Field Effect Transistor (SiC MOSFET) strengthen the parasitic inductances' impact onto the power module switching behavior. Thus, new multifunctional components that optimize the power module design are a promising field of research. For instance, the integration of capacitors into the module's packaging improves the switching's behavior [2]. Note that capacitors can deserve multiple purpose as energy storage or decoupling. Dang and Kwak [3] report the different kind of capacitors used in power electronics modules such as metallized polypropylene film capacitors, aluminum electrolytic capacitors and high capacitance multilayer ceramic capacitors The nature of the capacitor will drive its final use, *e.g*. decoupling of storage purposes. In the case of an embedded capacitor close to the switching device, decoupling capacitors are the most useful. Nevertheless, their adaptability to the integration processes, as their properties versus operating temperature and frequencies are key factors. Effectively, the use of a SiC MOSFET allows an increase of operating temperature, higher than 150°C, which makes ceramic capacitors the evident choice for integration purpose.

Contrary to usual studies where off the shelf capacitors are integrated into specific package design, our innovation deals with the co-design of a thick metalized ceramic, fully compatible with a power module integration process, and having a stable capacitor behavior in a reduced volume. In other words, to meet standard package, the integrated capacitor should replace the usual metalized ceramic substrate.

As a matter of facts, the ceramic capacitor must be miniaturized and positioned as close as possible of the power dies. According to the latter assumptions, an embedded ceramic capacitor including a thick metal (several hundred of µm) for its connection is needed. Moreover, the capacitor is developed to be compatible with a tin silver copper (SnAgCu) brazing process, and an ultrasonic to wire bonding connection. These latter materials are used to achieve the electrical connection between every active chip and its copper tracks. Indeed, the inner interconnection, thanks to wire bonding or large copper interconnects, will be insured, including integrated ceramic capacitor. The ideal ceramic size must be related to the backside area of the SiC MOSFET die used (~4*4 mm^2). To guarantee both thermal dissipation and geometry integration, its overall thickness will not be more than 2mm.

The assembly of metals and ceramics is a hard task due to the difference of thermal expansion coefficient, the temperature of manufacturing and eventually adhesion issues at the interface. Various ceramic-metal joining techniques have been improved and developed since the past century. The main methods are reactive metal brazing [4] or solid-state diffusion [5]. The final way is to co-sinter the two materials and create an adhesion between the surfaces of the materials. The main issue is to manage the stress created between the two materials, during the sintering process.

Barium titanate ($BaTiO_3$) ceramic was chosen as the dielectric material. Takeuchi et al. [6] have shown the excellent dielectric properties as high permittivity and low dielectric loss for capacitor application. Guillemet-Fritsch et al. [7] sintered nanometric particles of $BaTiO_3$ with Spark Plasma Sintering (SPS) followed by adapted annealing treatment leading to dense nanoceramics with colossal dielectric permittivity. Voisin et al. [8] optimized the annealing treatment after sintering, which allows to keep high permittivity (10^5) while reducing the dielectric losses.

In the second hand, different types of metal can be found on the top of the substrate or beneath power electronic components. Silver (Ag), nickel (Ni) and copper (Cu) are widely used as metals conductors in power electronics devices. Ceramics are mostly sintered at temperature higher than 1000°C. To imagine a co-sintering with a metal, Ni is good candidate due to its high fusion temperature (1453°C) unlike copper and silver with lower melting point, 1084°C and 962°C respectively. Zhao et al. [9] worked on the optimization of the ductility of nickel which is a positive point for stress accommodation and allows the shaping of ceramic-metal components in one-step. Preliminary results have ruled out sintering $BaTiO_3$ and Ni directly on top of each other, as the samples cracked. The use of a compositional gradient makes it possible to limit the stresses between materials, which is why this work focuses on two types of composites: cermets and Functionally Graded Materials (FGM). Cermets are a mixture of ceramic and metallic materials, homogenously dispersed as shown by Aramian et al. Aramian et al. (2020). Generally, the metallic component provides toughness and ductility, while the ceramic component provides hardness and wear resistance. FGMs are composed of two or more materials that are gradually varied in composition and/or microstructure along a specific direction as described by Madan and Bhowmick [11]. The purpose is to achieve a gradient in material properties, such as thermal expansion, strength, or elasticity. In this work, FGM with a composition gradient is targeted to obtain crack-free ceramic-metal component. The quality of the adhesion between the different layers is the key point for the success of the final assembly integrity. Functionally graded materials (FGMs) are driving a lot of interests because of the new open possibilities that they allow. Density gradient, microstructural gradient or composition gradient can be obtained. The composition gradient can be introduced in a wide variety of systems as ceramic/ceramic[12,13], metal/metal[14,15] or ceramic/metal systems[16]. The fields of FGMs applications are vast: biomedical[12,17] mechanical structure[18,19] or thermal applications[20,21], etc... Bahraminasab et al.[22] created an Al_2O_3/Ti FGM with high adhesion of the layers due to a reaction between the metal and the ceramics. Wei et al. Wei et al. (2022) manufactured a symmetrical W/Si_3N_4/W FGM and demonstrated that the number of layers was a predominant parameter to achieve a crack-free device. Only one article described FGM with $BaTiO_3$ and nickel. Saidani et al. Saidani et al. (2022) elaborated a $BaTiO_3$/Ni FGM with 5 layers, thanks to SPS sintering at 900°C. They obtained a good adhesion between layers and the mechanical properties of the $BaTiO_3$ and nickel were kept in the layers. To obtain the FGM structure, a gradient of composition is needed. Most of the FGM are obtained by powder metallurgy process. Nagarajan and Nicholson[25] created a continuous gradient by electrophoretic deposition but the easiest and most common way is to create a discontinuous FGM. For the gradient creation, different compositions of cermets are needed [11,16,26,27]. Once the composites are prepared, the materials are stacked in a mold before sintering. Spark Plasma Sintering (SPS) is a good path for FGM manufacturing because of the low sintering temperature, applied load and fast cycle.

In this work, the novelty is about the integrated ceramic capacitor design, from material choice and sintering process optimization to characterizations' methods, dedicated to power module's assembly. The feasibility of preparing an asymmetrical $BaTiO_3$/Ni FGM in one step, using SPS process, is demonstrated. The final FGM geometry is cylinders of 2 mm thickness and two different diameters, 8 mm and 15 mm. The thickness is chosen to help the feasibility of the device. The two different diameters allow to compare the dielectric properties and processing possibilities. The purpose of this work is to obtain a functionalized ceramic, with a capacitive behavior showing dielectrics properties close to the ones of a single phase $BaTiO_3$ that will be the ceramic substrate of the power module package. It should be suitable for integration in a power electronic device, thanks to the Ni thick layer. Firstly, the preparation of the sample is detailed. Secondly, the structure and the microstructure of the initial powders and of the dense FGM are described. Then, the dielectrical properties of the sample are presented. Finally, the possibility of integrating the component by brazing and wire-bonding is demonstrated.

II. EXPERIMENTAL PROCEDURE

A. Description of the capacitor

The FGM is composed of three materials: $BaTiO_3$, nickel and a ceramic-metal composite (cermet). The single layer of cermet is introduced between $BaTiO_3$ and nickel with a composition of 30% weight of nickel and 70% weight of $BaTiO_3$ (N3B7).

The volume ratio between the dielectric material $BaTiO_3$ and the metal nickel in the cermet is chosen to accommodate the stress. Moreover, the prepared capacitor should keep the interesting colossal permittivity ($>10^4$) as the one observed for pure $BaTiO_3$ as shown by Valdez-Nava et al.[28]. The thickness ratio between materials is chosen to maximize the integrity of the device. Fig. 1 shows the composition and the dimensions of the three layers of the FGM targeted. $BaTiO_3$, N3B7 and nickel layers are 0.5mm, 1mm and 0.5mm in thickness, respectively. The final layer of gold (100nm) is deposed using Physical Vapor Deposition (PVD).

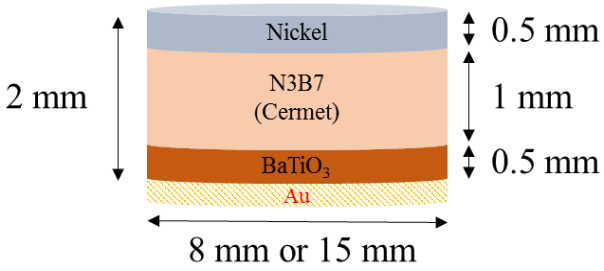

Fig. 1 Geometry and composition of the FGM

B. Powders

$BaTiO_3$ nanopowders were synthesized by a coprecipitation route. Laboratory made $TiOCl_2$ (15% weight of Ti) solution and, $BaCl_2$-$2H_2O$ (Prolabo, 99% purity) were used as precursors. The chlorides are dissolved in water and precipitated to an ethanol acid oxalic solution (Prolabo, 99% purity). The solution is stirred for 5h, centrifuged at 4200 rpm to separate the oxalate from the solution. It is dried at 80 °C and calcinated at 850°C to obtain the oxide. Voisin et al. [8] described the detailed protocol in a previous paper. The nickel thick layer, and the nickel used in the cermet are from the same manufacturer. The micronic nickel powders (Merck) has particle size of 3-7 µm and 99.8% purity. N3B7 composite is prepared with nickel and a $BaTiO_3$ powder (Marion Technologies) with 0.3-0.5 µm particles (BT_m), to avoid the use of synthetized $BaTiO_3$ (BT_s) in large scale. The powders are firstly merged manually, then mixed with a Turbula mixer during 4 h to obtain a good dispersion.

C. Sample preparation

The Spark Plasma Sintering process is achieved to get a dense FGM sample. The SPS device used, located at the Plateforme Nationale de Frittage Flash (PNF^2), is a Dr. Sinter 632Lx from Fuji Electronic Industrial CO, Japan. A graphite die (ISO68, Toyo Tanso) is used to receive the powders as well as to conduct the current that induces the heating. Based on the full density of each material, the calculated mass is introduced into the die for obtaining the right overall thickness (2 mm) of the sample. Let us remind that the sample is composed of three layers. The protocol used to place the different raw materials before applying the sintering profile is depicted in Fig. 2. Two pellets of alumina (thickness = 2 mm) are sintered at the same time at the bottom and the top of the FGM. The alumina and the sample are separated by a 0.2 mm graphite foil (PERMA-FOIL, Toyo Tanso). The alumina material and the graphite foil are entirely removed at the end of the process. The necessity to add alumina is discussed in the following. Before the placement of the raw materials, a graphite foil is placed on the total surface of the graphite die. As illustrated in Figure 2, the protocol is made of three steps. Step one (a) consists in placing a layer of alumina covered by graphite foil. The second step (b) consists in placing the other raw materials ($BaTiO_3$, N3B7 and Ni) and pressing the system after each

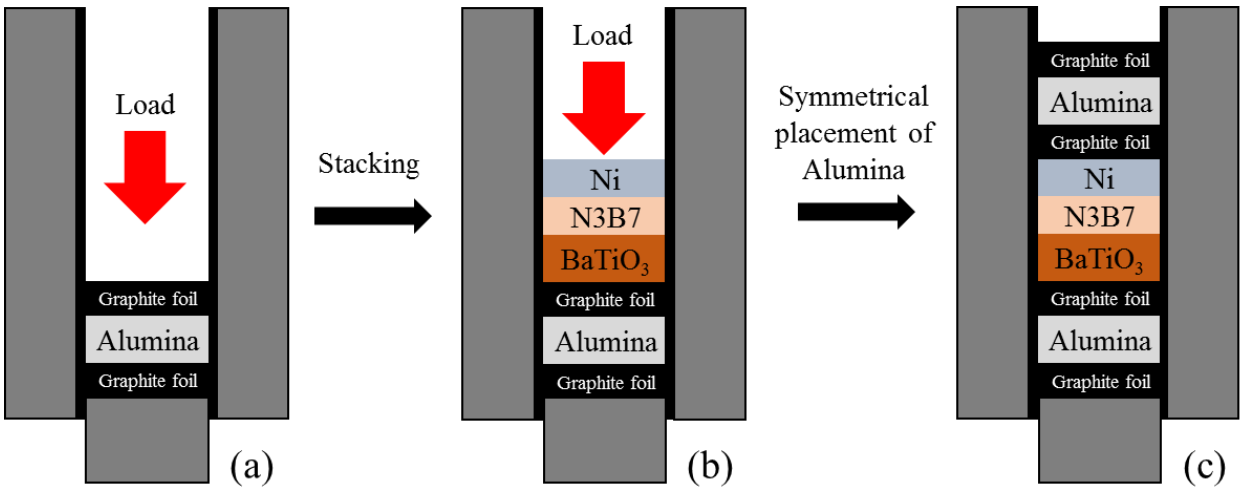

Fig. 2 Protocol of preparation of the graphite die before sintering

layer. Finally (c), a graphite foil is added and the last layer of alumina is placed. The quality of the stacking is determinant for the integrity of the final system.

D. Sintering behavior of FGM samples

The samples were sintered under vacuum environment (residual pressure < 20 Pa) with the sintering cycle shown in Fig. 3. The temperature is stabilized at 600 °C during 3min and the samples are heated to 1100 °C with a heating rate of 100 °C/min. A pressure of 25 MPa is applied at 1000 °C and held during 4 min. The dwell temperature is maintained for 5 min. Pressure is released and temperature decreased at 25°C/min. An optical pyrometer, focused on a hole (3 mm deep) at the external surface of the die, is used for monitoring the temperature during the sintering. The sintering parameters should be chosen with care to obtain a crack free device.

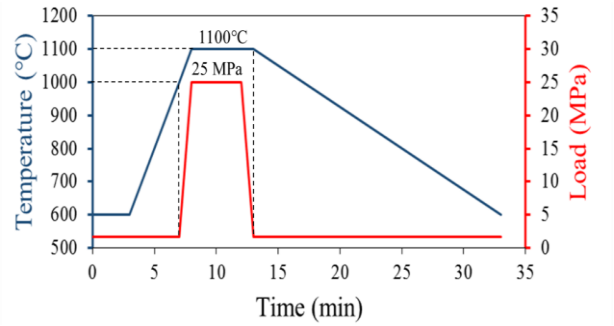

Fig. 3 Sintering cycle at 1100°C and 25MPa of the FGM sample

Figure 4 shows the corrected shrinkage behavior of the FGM, with and without alumina during sintering. When the FGM is sintered without the alumina pellets, the main part of shrinkage occurs before the temperature dwell. In another hand, it is clearly demonstrated that with the alumina, the shrinkage still increases during the temperature step and even during the beginning of the cooling. It is well known that metal and ceramics have different CTE that will create stress between the material during sintering and cooling. One role of alumina is to decrease additional stress. The first advantage of alumina is that its lack of density during sintering will accommodate mechanical stresses due to misalignment of the piston or defaults in the mold. Secondly, Manière et al.[29] reported that there is an increasing of the temperature at the junction between piston, graphite foil and the sample due to electrical contact resistance. Thence, the presence of the alumina isolates the FGM from the thermal gradient and allows the sample to be heated only by the Joule effect in the graphite die. As a matter of fact, crack-free $BaTiO_3$/Ni FGM with a diameter of 15 mm is obtained.

Guillemet-Fritsch et al.[7] have shown that after sintering, the $BaTiO_3$ appears in a dark blue color, due to the reduction of Ti^{4+} in Ti^{3+} cations. This color is also observed on the face of the FGM. This reduction is due to the oxygen poor environment of the SPS vacuumed chamber, combined with a graphite die. Therefore, the pellets were polished and annealed under oxidizing atmosphere at 850°C for 4 hours. The surface of $BaTiO_3$ is coated with 50nm gold obtained by Physical Vapor Deposition (PVD) (108 Auto Cressington Scientific Instruments). This layer provides the bottom metallized layer.

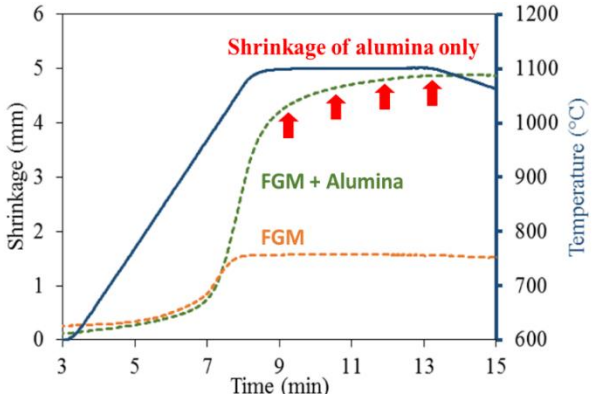

Fig. 4 Shrinkage of the FGM with or without alumina, and pure alumina

E. Characterizations

The morphology of the powders, the mapping composition of the pellets and the integrity of the system were analyzed with a scanning electron microscope (TESCAN Vega 3) coupled with an Oxford INCA Energy Dispersive Spectroscopy (EDS) detector using 20 kV acceleration voltage. Structural X-Ray Diffraction (XRD) analyzes of the pellets were performed with a Bruker D4 Endeavor diffractometer at room temperature with Cu $K\alpha_1$ and $K\alpha_2$ radiation in the range of 20° to 60° 2Θ angle. A cross-section

polisher JEOL (IB-19510CP) was used to cut-off the FGM sample with Focused argon Ion Beam (FIB). A SEM-FEG (FEI HELIOS 600i) microscope is used to look at the internal microstructure of the FGM. The relative permittivity and the dielectrical losses are obtained at room temperature after annealing 4h at 850°C from impedance spectroscopy measurement using a 4294A Precision Impedance Analyzer (Agilent Technologies) in the range 40 Hz - 1 M Hz and at room temperature.

III. RESULTS AND DISCUSSION

A. *Morphology of BT_m, nickel and N3B7 powders*

SEM FEG observations of the different powders are given in Fig. 5. The BT_m powder (Fig. 5(a)) shows rounded shape with average particle size of about 500 nm. The nickel particles present flower like shape, with size ranging from 1 to 5 µm (fig 5b). The difference of particles size between Ni and BT_m is a chosen parameter to prepare the FGM. Effectively, the large size of the nickel particles limits the probability of interaction between two particles, so avoiding percolation. Tuan and Chen[30] showed that the low particles interaction probability avoids a conduction path for the electrons in the future dense composite. The purpose is to obtain a ceramic matrix with dispersed metal in it with a chance to maximize the dielectrical properties of $BaTiO_3$[31,32]. Tuan and Chen [30] explained that the well weight ratio is chosen to limit the potential percolation path. A ratio of 30% is used here. The Fig. 5(c) shows the composite powder of N3B7 with a low magnification. The nickel particle at the center is surrounded by $BaTiO_3$ powder. The Fig. 5(d) is taken at a higher magnification and focus on the nickel particle. $BaTiO_3$ particles are coated onto the surface of nickel. The morphology and the size of nickel particle make easier the physical interaction between the two powders.

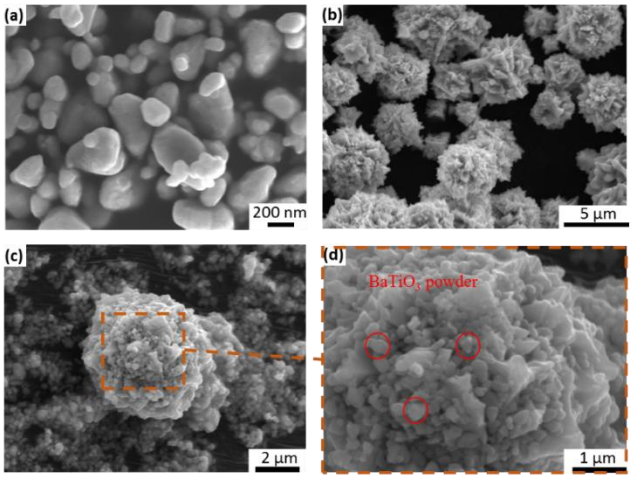

Fig. 5 SEM-FEG images of BT_m (a) nickel (b) and N3B7 powder (c, d)

B. *Microstructural and structural characterizations of the FGM*

To analyze the behavior of the materials after sintering, FGM sample are cut-off with a cross polisher to observe the microstructure of the FGM. Figure 6(a) shows the SEM-FEG image of N3B7 and Figure 6(b) the interface between nickel and N3B7 in the dense FGM. The backscattering electrons used for imaging reveals the nickel grain inside the BT_m matrix, as illustrated in Figure 6(a). The biggest particle of nickel has a size of 10 µm. So limited grain growth occurs during sintering. It can be explained by the fact that nickel particles are well distributed in the ceramic matrix. This leads to few contacts between Ni particles.

The diffusion between nickel grains is almost impossible so the grain growth is limited, even stopped. The bottom of Fig. 6(b) shows the interface of N3B7 and nickel at a higher magnification. An homogeneous distribution of the nickel particle (black spots) in the BT_m matrix can be observed in N3B7.The interface between nickel and N3B7 is straight, and well defined. The grain size of nickel in the nickel layer is higher than 100 µm, indicating grain growth in this case.

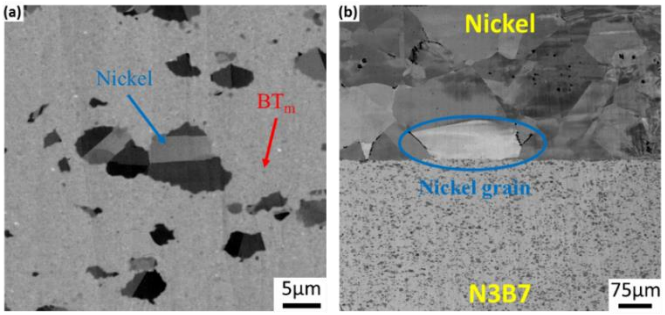

Fig. 6 SEM FEG micrographs showing the microstructure of the FGM in N3B7 (a) and at the interface between nickel and N3B7 (b)

Figure 7 depicts SEM images of the entire asymmetrical BT_s/N3B7/Ni FGM pellet sintered by SPS after cutting. The thicknesses targeted for the layers were respectively 500 µm, 1 mm and 500 µm for BT, N3B7 and Ni. To observe the different layers with a better contrast, backscattering electrons mode was used (Fig. 7 (a)). Since the final FGM thickness (1 mm) after sintering is the same as the targeted one, it is assumed that the material is close to full density. The image of Fig 7(b) shows no cracks. So, the observation of the overall sample (Fig 7 (c)) confirms the integrity of the FGM. A photography of the sample simple

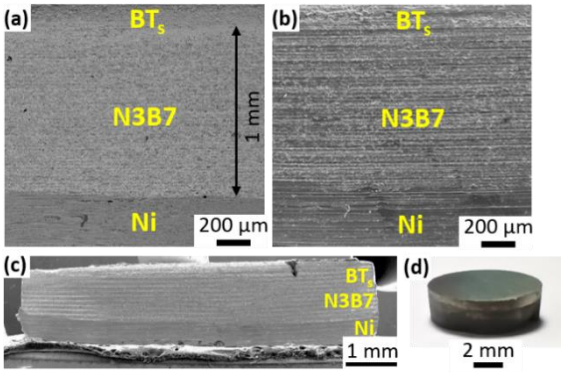

Fig. 7 SEM image of the 8 mm Ø asymmetrical BT_s/N3B7/Ni FGM sample, backscattering electron mode (a), secondary electron mode (b, c) and photo of the FGM (d)

before cutting is shown in Fig. 7(d).

EDS mapping of the surface of the sample shows the distribution of nickel, titanium, barium and oxygen (Fig. 8). The upper region is composed only with Ba, Ti and O as depicted in Fig. 8 (a, b). The lower region is composed with Ni and a small amount of oxygen as illustrated in Fig. 8 (c, d). With this analyze, it is concluded that no diffusion of the different materials occurs during the sintering. These analyses confirm that a homogenous asymmetrical FGM is obtained. One face is made of external face of pure $BaTiO_3$ and the opposite one with nickel. These macroscopic analyzes were completed by structural information on the different layers.

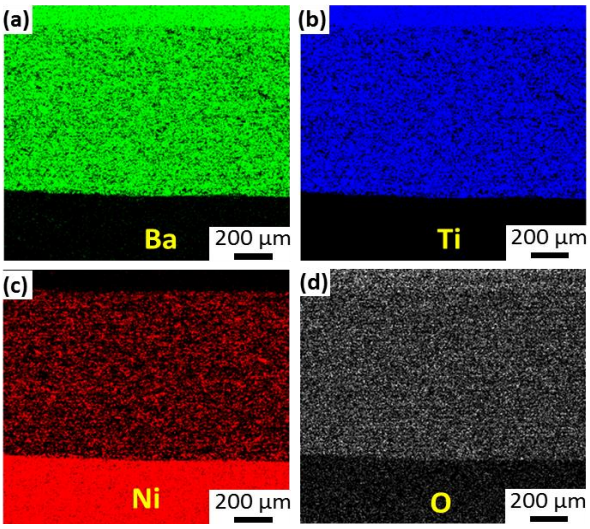

Fig. 8 EDS mapping of the 8mm Ø asymmetrical BT/N3B7/Ni FGM sample, barium distribution (a), titanium distribution (b), nickel distribution (c) and oxygen distribution (d)

Figure 9 presents the XRD of the different layers of materials of the FGM, after sintering (XRD of nickel face, BTs face). For comparison the XRD patterns of N3B7 and the BT_m are also shown. For this analysis, the N3B7 and BT_m were sintered separately by SPS with the same sintering cycle as the one used for the entire assembly and a thickness of 2 mm. The XRD of nickel face shows only one phase, the face-centered cubic nickel. The BT_s part presents a major phase of tetragonal barium titanium oxide and an additional phase, $Ba_4Ti_{12}O_{27}$ with the characteristic pic at 28.677°. The apparition of this phase is explained by the small excess of $TiOCl_2$ introduced during the coprecipitation. This titanium excess allows the formation of a secondary phase, $Ba_4Ti_{12}O_{27}$. Voisin et al.[8] showed the interest of this additional phase for improving the dielectric properties. On the contrary, the BT_m presents only the tetragonal $BaTiO_3$ phase. The cermet N3B7 (nickel and BT_m) is composed of two major phases which are cubic nickel and tetragonal $BaTiO_3$. It is shown that there is no phase formation between those two compounds, and that no reaction occurred during sintering. The structural and microstructural characterizations both demonstrate the homogeneity of the FGM. The dielectric properties (permittivity and losses) are detailed in the following.

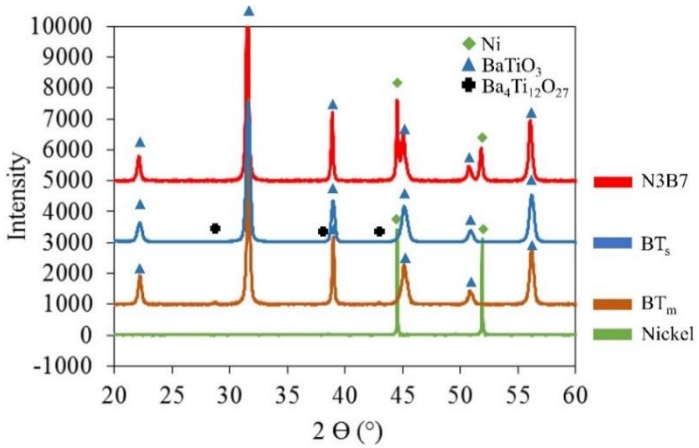

Fig. 9 XRD of nickel, BTs, BTm and N3B7 after sintering

C. Dielectric properties of the FGM

In this work, the composition of the composite layer has been chosen for improving the electrical properties of $BaTiO_3$. Indeed, the ratio of 30% weight of nickel corresponds to a volume ratio of 22%. In the literature, some papers report on dielectric constant increase when nickel is added to $BaTiO_3$ if the volume ratio of nickel is under 31%[31,33,34]. At the percolation threshold an increase of permittivity is observed. Past this value the material behaves as a conductive material. In these papers the nickel and the $BaTiO_3$ particles have nanometric size and the sintering process is realized under argon or nitrogen atmosphere. In our case, the use of graphite die in a vacuum atmosphere lead to a poor oxygen environment during SPS sintering. Yoon et al. [35] reported on the conduction mechanism in $BaTiO_3$-Ni composites sintered by SPS, without further annealing after sintering. These

authors indicated that the conductivity of the $BaTiO_3$-Ni cermet increases with the Ni content, and that the value of the conductivity value is significantly higher than the one of $BaTiO_3$ sintered conventionally. In our study the composite (N3B7) placed between Ni and $BaTiO_3$ in the FGM cannot be fully reoxidize because the oxygen diffusion is limited to the material on the top and beneath. We don't want a total reoxidization of the system because Emoto and Hojo [36] shown that the formation of NiO would decrease the permittivity and increase dielectric losses.

The Figure 10 shows the relative permittivity and the dielectric losses of nine BaTiO3/Ni FGMs 15mm pellets sintered by SPS and annealed under the same conditions. All the samples present colossal permittivity (~10^5), low dielectric losses (>10%) which are stable up to 10^4 Hz. Above this frequency, relaxation occurs, and the losses increase as permittivity decreases. The dielectric behavior of the FGMs are close in frequency.

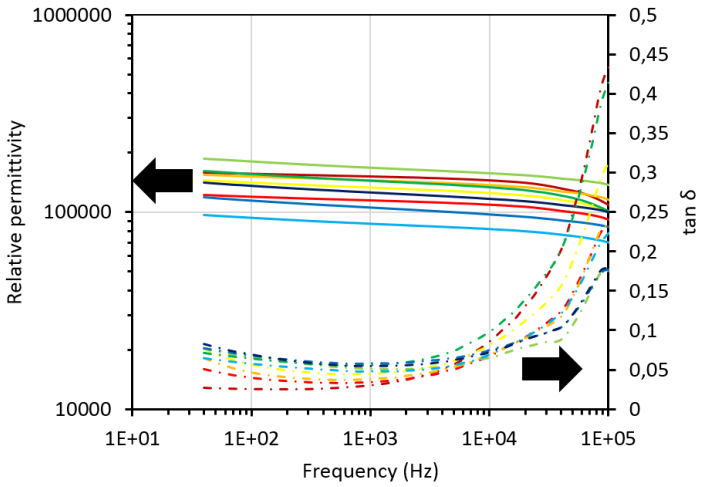

Fig 10 Relative permittivity and tan δ in frequency of nine $BaTiO_3$/Ni FGMs

Table I shows the capacity, permittivity and dielectric losses values of the nine BaTiO3 FGMs of 15mm diameter at a frequency of 1 kHz. The FGMs have low dielectric losses between 3,0 % and 5.8 % with an average at 4,6±1,0 %, a permittivity between $8{,}7.10^4$ and $1{,}7.10^5$ with an average of $1{,}31{\pm}0{,}25.10^5$. The capacitance is between 70 nF and 137 nF with an average at 108±22 nF. These results confirm the reproducibility of dielectric properties for samples of identical composition, sintered and annealed under the same conditions. The capacitor prepared in this work keep the interesting colossal permittivity (>10^4) and low losses as the one of pure $BaTiO_3$ as shown by Valdez-Nava et al. [28]. The Cermet layer have no impact on the dielectric properties of the sample. These properties highlight the fact that even with a complex system, the dielectric properties of $BaTiO_3$ remain interesting, even when integrated in a multi-layer system with alternative properties. Such FGM with this composition and properties has never been reported in the literature.

Table I Dielectric properties of the nine $BaTiO_3$/Ni FGMs (f = 1 kHz) of 15 mm

Frequency = 1 kHz

	FGM1	FGM2	FGM3	FGM4	FGM5	FGM6	FGM7	FGM8	FGM9
Capacity (nF)	130	95	126	106	137	117	70	88	105
Permittivity	152120	114765	144805	132884	167986	144298	87305	105820	126123
Dielectric losses (%)	3,0	3,4	3,8	4,5	5,0	5,6	4,8	5,8	5,4

Figure 11 is a schematic representation of the $BaTiO_3$ layer in the FGM after the annealing at 850 °C. As reported in previous work [8], only the external surface of the sample is oxidized after the annealing treatment. The external surface of the sample plays a key role for the dielectric properties of the FGM. The dielectric behavior of the overall FGM system is probably the same as the one we reported for pure $BaTiO_3$ [37], i.e. a combination of internal barrier layer capacitance (IBLC), electron-pinned defect-dipole (EPDD) and surface barrier layer capacitance (SBLC). Voisin et al. [8] claimed that the colossal permittivity of BT_s was due to ~15% of electrode effect, ~20% of interfacial polarization and ~65% of hopping polarization. The Cermet layer here seems to have no impact on the dielectric properties of the sample.

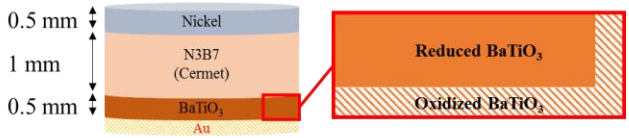

Fig. 11 Behaviour of the $BaTiO_3$ layer of the FGM after annealing

IV. TOWARDS FGM INTEGRATION

The goal of this work is to create a device that can be integrated in a power-module. The figure 12 shows the FGM brazed on ceramic substrate with nickel metallization. Wire bonding are interconnected from the top of the FGM to the metalized substrate. The bonding with the surface of the FGM is a success and shows the possibility of integration of this device in a power assembly. Thirty wires (Ø 150 µm) were bonded to the surface of a $BaTiO_3$/Ni FGM. Pull-test tests were carried out on these wires and 90% of the wires broke at the top of the wire loops with an average strength of 127 gf. This demonstrates good adhesion of the wires to the Ni. After the wires broke, no signs of delamination were observed. This experiment established that this sample has good compatibility for power electronic integration.

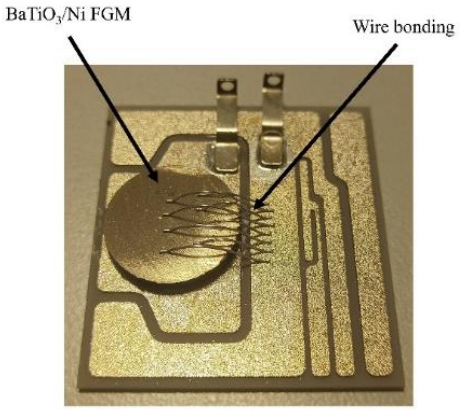

Fig. 12 $BaTiO_3$ FGM brazed on a substrate with wire bonding interconnexions

V. CONCLUSION

In this preliminary study for having functionalized ceramic dedicated to power module design, we optimized single step processing to obtain an asymmetrical $BaTiO_3$/nickel FGM with three layers, coupled with sacrificial alumina. The powder synthesis, the cermet preparation and the sintering parameters allow to create a dense metal/ceramic crack-free FGM with controlled microstructure and without parasite interdiffusion reaction. The overall pellet has similar dielectric properties to the ones of pure $BaTiO_3$ sintered by SPS. It is shown that the thick nickel metallization allows a new function leading to new assembly possibilities in power module design. Future works will focus on tree topics: mechanical test of the interface and brazed component, dielectrical breakdown test and thermal cycling of the devise to see if it can stand high voltage (≥1kV) and high operating temperature (≥200°C).

VI. ACKNOWLEDGMENTS

This work is supported by the funding PIA-ANR-16-IDEX-0002, project Energy And Solution for Environment - E2S UPPA within the framework of the EFFICIENCE Chaire. The authors are grateful to C. Josse for the SEM images after cross polishing.

VII. REFERENCES

[1] E. Santi, S. Eskandari, B. Tian, K. Peng, "6 - Power Electronic Modules"*Butterworth-Heinemann*, 2018: pp. 157–173. https://doi.org/10.1016/B978-0-12-811407-0.00006-4.

[2] B. Whitaker, Z. Cole, B. Passmore, D. Martin, T. McNutt, A. Lostetter, M.N. Ericson, S.S. Frank, C.L. Britton, L.D. Marlino, A. Mantooth, M. Francis, R. Lamichhane, P. Shepherd, M. Glover, "High-temperature SiC power module with integrated SiC gate drivers for future high-density power electronics applications"2014: pp. 36–40. https://doi.org/10.1109/WiPDA.2014.6964620.

[3] H.-L. Dang, S. Kwak, "Review of Health Monitoring Techniques for Capacitors Used in Power Electronics Converters," *Sensors*. 20 (2020) 3740. https://doi.org/10.3390/s20133740.

[4] S. Mishra, A. Sharma, D.H. Jung, J.P. Jung, "Recent Advances in Active Metal Brazing of Ceramics and Process," *Met. Mater. Int.* 26 (2020) 1087–1098. https://doi.org/10.1007/s12540-019-00536-4.

[5] S. Das, A.N. Tiwari, A.R. Kulkarni, "Thermo-compression bonding of alumina ceramics to metal," *Journal of Materials Science*. 39 (2004) 3345–3355. https://doi.org/10.1023/B:JMSC.0000026935.18466.4b.

[6] T. Takeuchi, Y. Suyama, D.C. Sinclair, H. Kageyama, "Spark-plasma-sintering of fine BaTiO3 powder prepared by a sol-crystal method," *Journal of Materials Science*. 36 (2001) 2329–2334. https://doi.org/10.1023/A:1017585209648.

[7] S. Guillemet-Fritsch, Z. Valdez-Nava, C. Tenailleau, T. Lebey, B. Durand, J.-Y. Chane-Ching, "Colossal Permittivity in Ultrafine Grain Size BaTiO3–x and Ba0.95La0.05TiO3–x Materials," *Advanced Materials*. 20 (2008) 551–555. https://doi.org/10.1002/adma.200700245.

[8] C. Voisin, S. Guillemet-Fritsch, P. Dufour, C. Tenailleau, H. Han, J.C. Nino, "Influence of Oxygen Substoichiometry on the Dielectric Properties of BaTiO3-δ Nanoceramics Obtained by Spark Plasma Sintering," *International Journal of Applied Ceramic Technology*. 10 (2013) E122–E133. https://doi.org/10.1111/ijac.12058.

[9] Y. Zhao, T. Topping, J.F. Bingert, J.J. Thornton, A.M. Dangelewicz, Y. Li, W. Liu, Y. Zhu, Y. Zhou, E.J. Lavernia, "High Tensile Ductility and Strength in Bulk Nanostructured Nickel," *Advanced Materials*. 20 (2008) 3028–3033. https://doi.org/10.1002/adma.200800214.

[10] A. Aramian, S.M.J. Razavi, Z. Sadeghian, F. Berto, "A review of additive manufacturing of cermets," *Additive Manufacturing*. 33 (2020) 101130. https://doi.org/10.1016/j.addma.2020.101130.

[11] R. Madan, S. Bhowmick, "A review on application of FGM fabricated using solid-state processes," *Advances in Materials and Processing Technologies*. 6 (2020) 608–619. https://doi.org/10.1080/2374068X.2020.1731153.

[12] M.A.F. Afzal, P. Kesarwani, K.M. Reddy, S. Kalmodia, B. Basu, K. Balani, "Functionally graded hydroxyapatite-alumina-zirconia biocomposite: Synergy of toughness and biocompatibility," *Materials Science and Engineering: C*. 32 (2012) 1164–1173. https://doi.org/10.1016/j.msec.2012.03.003.

[13] E. Bódis, M. Jakab, K. Bán, Z. Károly, "Functionally Graded Al2O3–CTZ Ceramics Fabricated by Spark Plasma Sintering," *Materials*. 15 (2022) 1860. https://doi.org/10.3390/ma15051860.

[14] R. Ghanavati, H. Naffakh-Moosavy, "Additive manufacturing of functionally graded metallic materials: A review of experimental and numerical studies," *Journal of Materials Research and Technology*. 13 (2021) 1628–1664. https://doi.org/10.1016/j.jmrt.2021.05.022.

[15] M. Nemat-Alla, M.H. Ata, M.R. Bayoumi, W. Khair-Eldeen, "Powder Metallurgical Fabrication and Microstructural Investigations of Aluminum/Steel Functionally Graded Material," *Materials Sciences and Applications*. (2011). https://doi.org/10.4236/MSA.2011.212228.

[16] M. Tokita, "Development of Large-Size Ceramic/Metal Bulk FGM Fabricated by Spark Plasma Sintering," *MSF*. 308–311 (1999) 83–88. https://doi.org/10.4028/www.scientific.net/MSF.308-311.83.

[17] C. Chenglin, Z. Jingchuan, Y. Zhongda, W. Shidong, "Hydroxyapatite–Ti functionally graded biomaterial fabricated by powder metallurgy," *Materials Science and Engineering: A*. 271 (1999) 95–100. https://doi.org/10.1016/S0921-5093(99)00152-5.

[18] X. Qian, D. Dutta, "Design of heterogeneous turbine blade," *Computer-Aided Design*. 35 (2003) 319–329. https://doi.org/10.1016/S0010-4485(01)00219-6.

[19] A. Reichardt, A.A. Shapiro, R. Otis, R.P. Dillon, J.P. Borgonia, B.W. McEnerney, P. Hosemann, A.M. Beese, "Advances in additive manufacturing of metal-based functionally graded materials," *International Materials Reviews*. 66 (2021) 1–29. https://doi.org/10.1080/09506608.2019.1709354.

[20] M. Bhattacharyya, A.N. Kumar, S. Kapuria, "Synthesis and characterization of Al/SiC and Ni/Al2O3 functionally graded materials," *Materials Science and Engineering: A*. 487 (2008) 524–535. https://doi.org/10.1016/j.msea.2007.10.040.

[21] X. Jin, L. Wu, Y. Sun, L. Guo, "Microstructure and mechanical properties of ZrO2/NiCr functionally graded materials," *Materials Science and Engineering: A*. 509 (2009) 63–68. https://doi.org/10.1016/j.msea.2009.01.066.

[22] M. Bahraminasab, S. Ghaffari, H. Eslami-Shahed, "Al2O3-Ti functionally graded material prepared by spark plasma sintering for orthopaedic applications," *Journal of the Mechanical Behavior of Biomedical Materials*. 72 (2017) 82–89. https://doi.org/10.1016/j.jmbbm.2017.04.024.

[23] Z. Wei, S. Liu, D. Liu, J. Wu, H. Xia, B. Wang, Z. Shi, "Fabrication and properties of symmetrical W/Si3N4/W functionally graded materials by spark plasma sintering," *Journal of Alloys and Compounds*. 896 (2022) 163077. https://doi.org/10.1016/j.jallcom.2021.163077.

[24] B. Saidani, J. Cedelle, J. Petit, D. Bregiroux, J. Zghal, I. Bruant, “Caractérisation expérimentale des propriétés physiques et mécaniques de FGPM Ni/BaTiO₃”*Nantes, France*, 2022. https://hal.archives-ouvertes.fr/hal-03768978 (accessed October 5, 2022).

[25] N. Nagarajan, P.S. Nicholson, “Nickel–Alumina Functionally Graded Materials by Electrophoretic Deposition,” *Journal of the American Ceramic Society*. 87 (2004) 2053–2057. https://doi.org/10.1111/j.1151-2916.2004.tb06359.x.

[26] F. Casari, M. Zadra, L. Girardini, A. Molinari, “Development of Al2O3-Ni FGMs Produced by Spark Plasma Sintering,” *Proceedings of the Korean Powder Metallurgy Institute Conference*. (2006) 87–88.

[27] A. Pasha, R. B.m, “Functionally graded materials (FGM) fabrication and its potential challenges & applications,” *Materials Today: Proceedings*. 52 (2022) 413–418. https://doi.org/10.1016/j.matpr.2021.09.077.

[28] Z. Valdez-Nava, S. Guillemet-Fritsch, Ch. Tenailleau, T. Lebey, B. Durand, J.Y. Chane-Ching, “Colossal dielectric permittivity of BaTiO3-based nanocrystalline ceramics sintered by spark plasma sintering,” *J Electroceram*. 22 (2009) 238–244. https://doi.org/10.1007/s10832-007-9396-8.

[29] C. Manière, A. Pavia, L. Durand, G. Chevallier, K. Afanga, C. Estournès, “Finite-element modeling of the electro-thermal contacts in the spark plasma sintering process,” *Journal of the European Ceramic Society*. 36 (2016) 741–748. https://doi.org/10.1016/j.jeurceramsoc.2015.10.033.

[30] W.H. Tuan, S.S. Chen, “Processing and Properties of BaTiO3-Ni Ferroelectric-Ferromagnetic Composites,” *Ferroelectrics*. 381 (2009) 167–175. https://doi.org/10.1080/00150190902876090.

[31] C. Pecharromán, F. Esteban-Betegón, J.F. Bartolomé, S. López-Esteban, J.S. Moya, “New Percolative BaTiO3–Ni Composites with a High and Frequency-Independent Dielectric Constant (ϵr ≈ 80000),” *Advanced Materials*. 13 (2001) 1541–1544. https://doi.org/10.1002/1521-4095(200110)13:20<1541::AID-ADMA1541>3.0.CO;2-X.

[32] S. Yoon, J. Dornseiffer, T. Schneller, D. Hennings, S. Iwaya, C. Pithan, R. Waser, “Percolative BaTiO3–Ni composite nanopowders from alkoxide-mediated synthesis,” *Journal of the European Ceramic Society*. 30 (2010) 561–567. https://doi.org/10.1016/j.jeurceramsoc.2009.06.024.

[33] C. Pecharromán, F. Esteban-Betegón, R. Jiménez, “Electric Field Enhancement and Conduction Mechanisms in Ni/BaTiO3 Percolative Composites,” *Ferroelectrics*. 400 (2010) 81–88. https://doi.org/10.1080/00150193.2010.505478.

[34] M. Saleem, I.S. Kim, J.S. Song, S.J. Jeong, M.S. Kim, S. Yoon, “Synthesis, sintering and dielectric properties of a BaTiO3–Ni composite,” *Ceramics International*. 40 (2014) 7329–7335. https://doi.org/10.1016/j.ceramint.2013.12.075.

[35] S. Yoon, C. Pithan, R. Waser, J. Dornseiffer, Y. Xiong, D. Grüner, Z. Shen, S. Iwaya, “Electronic Conduction Mechanisms in BaTiO3–Ni Composites with Ultrafine Microstructure Obtained by Spark Plasma Sintering,” *Journal of the American Ceramic Society*. 93 (2010) 4075–4080. https://doi.org/10.1111/j.1551-2916.2010.04011.x.

[36] H. Emoto, J. Hojo, “Sintering and Dielectric Properties of BaTiO3-Ni Composite Ceramics,” *J. Ceram. Soc. Japan*. 100 (1992) 555–559. https://doi.org/10.2109/jcersj.100.555.

[37] H. Han, C. Voisin, S. Guillemet-Fritsch, P. Dufour, C. Tenailleau, C. Turner, J.C. Nino, “Origin of colossal permittivity in BaTiO3 via broadband dielectric spectroscopy,” *Journal of Applied Physics*. 113 (2013) 024102. https://doi.org/10.1063/1.4774099.